RESEARCH ARTICLE

Methamphetamine regulation of activity and topology of ventral midbrain networks

Douglas R. Miller[ORCID][1], Joseph J. Lebowitz[1], Dylan T. Guenther[ORCID][1], Alexander J. Refowich[1], Carissa Hansen[1], Andrew P. Maurer[1,2,3,4]*, Habibeh Khoshbouei[1]*

1 Department of Neuroscience, University of Florida, Gainesville, FL, United States of America, **2** McKnight Brain Institute, University of Florida, Gainesville, FL, United States of America, **3** Department of Biomedical Engineering, University of Florida, Gainesville, FL, United States of America, **4** Department of Civil and Coastal Engineering, University of Florida, Gainesville, FL, United States of America

* drewmaurer@ufl.edu (APM); habibeh@ufl.edu (HK)

Abstract

The ventral midbrain supports a variety of functions through the heterogeneity of neurons. Dopaminergic and GABA neurons within this region are particularly susceptible targets of amphetamine-class psychostimulants such as methamphetamine. While this has been evidenced through single-neuron methods, it remains unclear whether and to what extent the local neuronal network is affected and if so, by which mechanisms. Both GABAergic and dopaminergic neurons were heavily featured within the primary ventral midbrain network model system. Using spontaneous calcium activity, our data suggest methamphetamine decreased total network output via a D_2 receptor-dependent manner. Over culture duration, functional connectivity between neurons decreased significantly but was unaffected by methamphetamine. However, across culture duration, exposure to methamphetamine significantly altered changes in network assortativity. Here we have established primary ventral midbrain networks culture as a viable model system that reveals specific changes in network activity, connectivity, and topology modulation by methamphetamine. This network culture system enables control over the type and number of neurons that comprise a network and facilitates detection of emergent properties that arise from the specific organization. Thus, the multidimensional properties of methamphetamine can be unraveled, leading to a better understanding of its impact on the local network structure and function.

Introduction

The ventral midbrain neurons are one of the main targets of amphetamines. Amphetamine-class drugs have been shown to increase extracellular dopamine levels by stimulation of firing activity of dopamine neurons and via stimulation of dopamine efflux through the dopamine transporter [1]. Once in the extracellular space, dopamine rapidly diffuses from the site of release and acts upon both pre- and postsynaptic receptors [2–4]. Activation of presynaptic D_2 receptors in turn decreases firing activity of dopaminergic neurons and activation of postsynaptic D_2 receptors decreases postsynaptic neuronal activity [5]. Importantly, the majority of

ventral midbrain neurons are non-dopaminergic neurons [6], but many of which express D_2 receptors [7] that are modulated secondary to methamphetamine stimulation of dopamine release. While these effects have been extensively investigated in individual neurons, it remains unexplored how these activities affect the functional connectivity and topological network features.

Network analysis provides the necessary tools to determine how patterns emerge from paired neuronal activity, how they segregate and integrate information, and how specific regional composition and conditions predispose the network to failure [8–11]. For instance, in a previous study, neurons were plated in the absence of adhesion proteins, forcing neurons to grow in dense clusters. The activity of the dense clusters persisted in the presence of an excitatory neurotransmission inhibitor, or when neurons were exposed to light radiation. The observed persistence in dense clusters was contrasted to observations of cultures where the spatial distribution of neurons was homogenous, and activity decayed quickly under both conditions. In the clustered cultures, the networks were positively assortative while the homogenous cultures were approximately neutral, similar to other studies of cultured cortical networks [12,13]. Network analysis has also revealed unique signatures in hippocampal slices. In both acute and cultured hippocampal slice networks, gamma-aminobutyric acid (GABA) neurons function as network hubs, which orchestrate network synchrony [14,15]. The advantages of network science approaches can therefore be leveraged to investigate whether ventral midbrain network topology changes over time in culture or restructures during methamphetamine exposure.

GABA neurons are the major inhibitory interneurons in the ventral midbrain [16]. These neurons both project within and outside of the ventral midbrain. Unlike dopaminergic neurons, the basal physiological properties of GABAergic neurons are less understood [7]. Nevertheless, they are implicated in methamphetamine-mediated responses [17,18]. Previous work showed that following a single injection of methamphetamine, ventral midbrain GABA neurons exhibited depression of $GABA_B$ receptor signaling [18]. Furthermore, previous studies in organotypic hippocampal culture and acute cortical slices showed that exposure to neuromodulators such as acetylcholine or domoic acid inhibition of GABA neurons was sufficient to disrupt and reorganize network connectivity [19,20]. However, it is unclear whether the activity of GABA neurons, their functional connectivity, and/or network topology is altered during methamphetamine exposure. This study is aimed to uncover the mechanisms by which the functional connectivity and structure of cultured GABAergic networks is modulated by methamphetamine. Our goal is to establish a standard methodology to investigate neuronal network topology and to use this model to determine how methamphetamine regulates ventral midbrain network activity.

In this study, we have exploited spontaneous calcium activity, a proxy of neuronal activity [21], to determine the functional connectivity and network topology of ventral midbrain network culture. We determined how methamphetamine dysregulates network activity and impacts topological measurements, which can provide clues on how methamphetamine modulation of neuronal activity regulates functional connectivity relationships and topology of ventral midbrain neuronal networks. Our work represents the first investigation, to our knowledge, into the basal network topology of the ventral midbrain with single neuron resolution and further demonstrates the multitude of effects by methamphetamine from individual neurons to the constellation of the local network.

Results and discussion

Overview of network analysis and metrics in this study

Methamphetamine is a highly addictive drug that increases intracellular calcium concentration to modulate neuronal activity [22]. How methamphetamine modulates the communication

across neurons in a network is unclear. To determine how methamphetamine-modulation of single neurons affects functional connectivity relationships and topology of ventral midbrain neuronal networks, we employed network analysis. Functional connectivity between two neurons was defined as correlated activity [23] measured by the Spearman's rank correlation [12]. Functional connectivity was then used to calculate network density, clustering coefficient, modularity, and assortativity as representative metrics before and during methamphetamine exposure. Density is defined as the fraction of actual connections relative to total possible connections [9]. Clustering coefficient extends upon pair-wise correlations by determining the fraction of complete triangular connections around a neuron. Clustering coefficient is commonly applied to represent patterns of connectivity not evident from pair-wise correlations [24–26]. To identify the potential existence of individual subnetworks within the larger neuronal network, the modularity index (Q) was calculated. Finally, it has been shown that network topology may confer susceptibility to loss of critical nodes [9,12]. Therefore, we calculated assortativity as a general estimate of network resiliency. In general, a positive assortativity refers to preferential connectivity of neurons with similar connectivity [10]. For example, neurons with 10 connections are more likely to be connected to other neurons with multiple connections rather than those with a few connections. Negative assortativity is conventionally characterized by preferential connectivity to neurons with dissimilar connectivity [10]. For instance, neurons with 10 connections are more likely to be connected to neurons with 1 to 2 connections. Therefore, in certain situations, positive assortativity confers resiliency of the network, which enables compensation following neuronal loss (Fig 1).

Construction and characterization of ventral midbrain neuronal networks

To determine methamphetamine regulation of ventral midbrain neuronal networks culture, ventral midbrain was extracted from P0-P1 C57B6/J mice and transduced with the GCaMP6f transgene under a general neuronal promoter (Fig 2A). We monitored spontaneous calcium activity in a 10x field of view at 10 Hz (Fig 2B). Neuronal cell bodies were manually segmented and spontaneous calcium activity of GCaMP6f expressing neurons was extracted in order to calculate functional connectivity between neurons (Fig 2C and 2D). Symmetrical undirected adjacency matrices that represent co-active neurons were generated using the Spearman's rank correlation coefficient (Spearman's rho) of calcium activity signals before and during methamphetamine exposure (Fig 2E). Proportional thresholds were applied to isolate and explore the strongest 15% of functional connections and network topology at baseline and during methamphetamine exposure (Fig 2F). Connections surviving the threshold are then projected onto the recording to investigate the spatial location of the connected neurons (Fig 2G). Surprisingly, the strongest connections were not spatially localized but rather comprised by both proximal and distal neurons.

The ventral midbrain is a heterogeneous region comprised of neurons that vary in their neurotransmitter content and protein expression [7]. Therefore, we first quantified the ventral midbrain neuronal network cultures for the presence of tyrosine hydroxylase (TH, the rate-limiting enzyme of dopamine synthesis), gamma-aminobutyric acid (GABA), and HuC/D (an RNA-binding protein, as a pan-neuronal marker) (Fig 3A). TH labelling revealed that dopaminergic neurons, a direct target of methamphetamine, comprise approximately 12% of the total neural network (relative to HuC/D), with the remaining neurons being predominantly GABAergic (Fig 3B). These GABAergic neurons are one of the main targets of the released dopamine from dopaminergic neurons during methamphetamine exposure. Ventral midbrain neurons have been extensively characterized at the single neuron level [27–30], but there is no established standard for studying ventral midbrain neuronal networks under basal condition
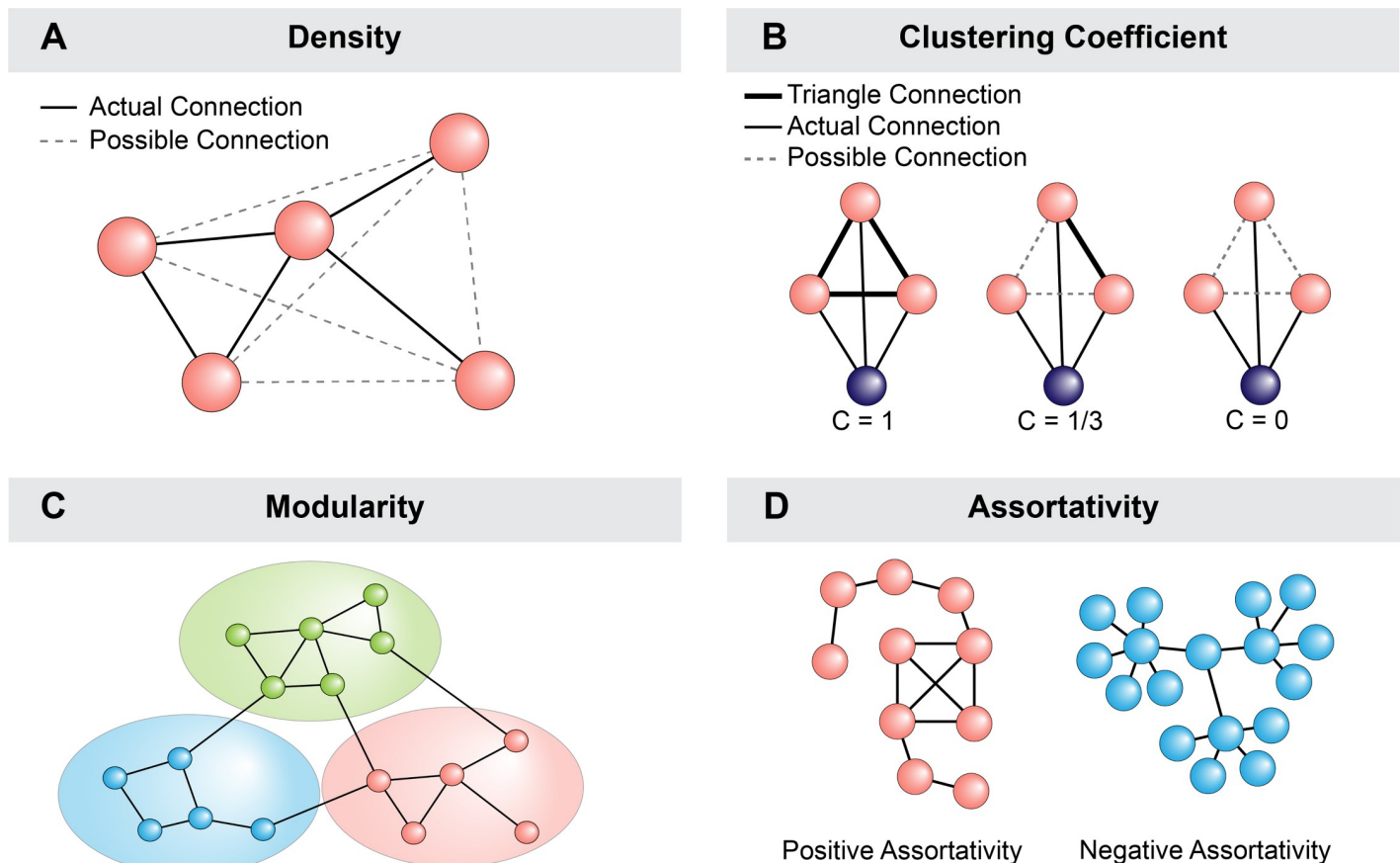
Fig 1. Overview of network metrics. This study utilizes network calculations of density, clustering coefficient, modularity and assortativity. (A) Density represents the actual connections to the total possible connections. Real-world networks are typically sparsely connected, conferring a low density. (B) Clustering coefficient determines the interconnectedness around each neuron by measuring the fraction of complete triangle connections. This metric extends from pair-wise connections to connectivity patterns that have implications on information propagation. (C) Modularity extends upon clustering by segregating the network into subgroups of high interconnectedness. Increases or decreases in modularity index are indicative of changes in community structure. (D) Assortativity evaluates preferential attachment between neurons of similar connectivity (positive) or dissimilar (negative).

and during methamphetamine exposure. Therefore, to establish a standard methodology for network analysis *in vitro*, the experiments and analysis were performed across development (nine to twenty-one days of neuronal network culture). We found the majority of neurons (~84%, mean HuC/D = 4085 ± 1419, mean GCaMP6f = 3426 ± 507) express GCaMP6f were similar amongst experimental groups and across development (denoted by Days *In Vitro* (DIV) Fig 4A and 4B). As we were interested in the temporal relationship between DIV and network dynamics, we first controlled for the temporal relationship between DIV and the number of recorded neurons per experimental group. Therefore, we assessed this relationship using simple linear regression and found no significant relationship (n = 3 independent replicates per DIV, p = 0.0916, r^2 = 0.08383), even when DIV is treated as categorical and assessed through one-way ANOVA (n = 3 independent replicates per DIV, p = 0.1378, F (11, 23) = 1.695) (Fig 4C). These data establish a reliable model system that can be employed to examine the functional connectivity and topology of ventral midbrain neuronal networks culture and stem cell-derived human neuronal networks. By establishing this model, it will be possible to relate how the dysfunction of a single neuron can establish pathological spreading of dysfunction that is believed to underlie disorders of the ventral midbrain such as Parkinson's disease
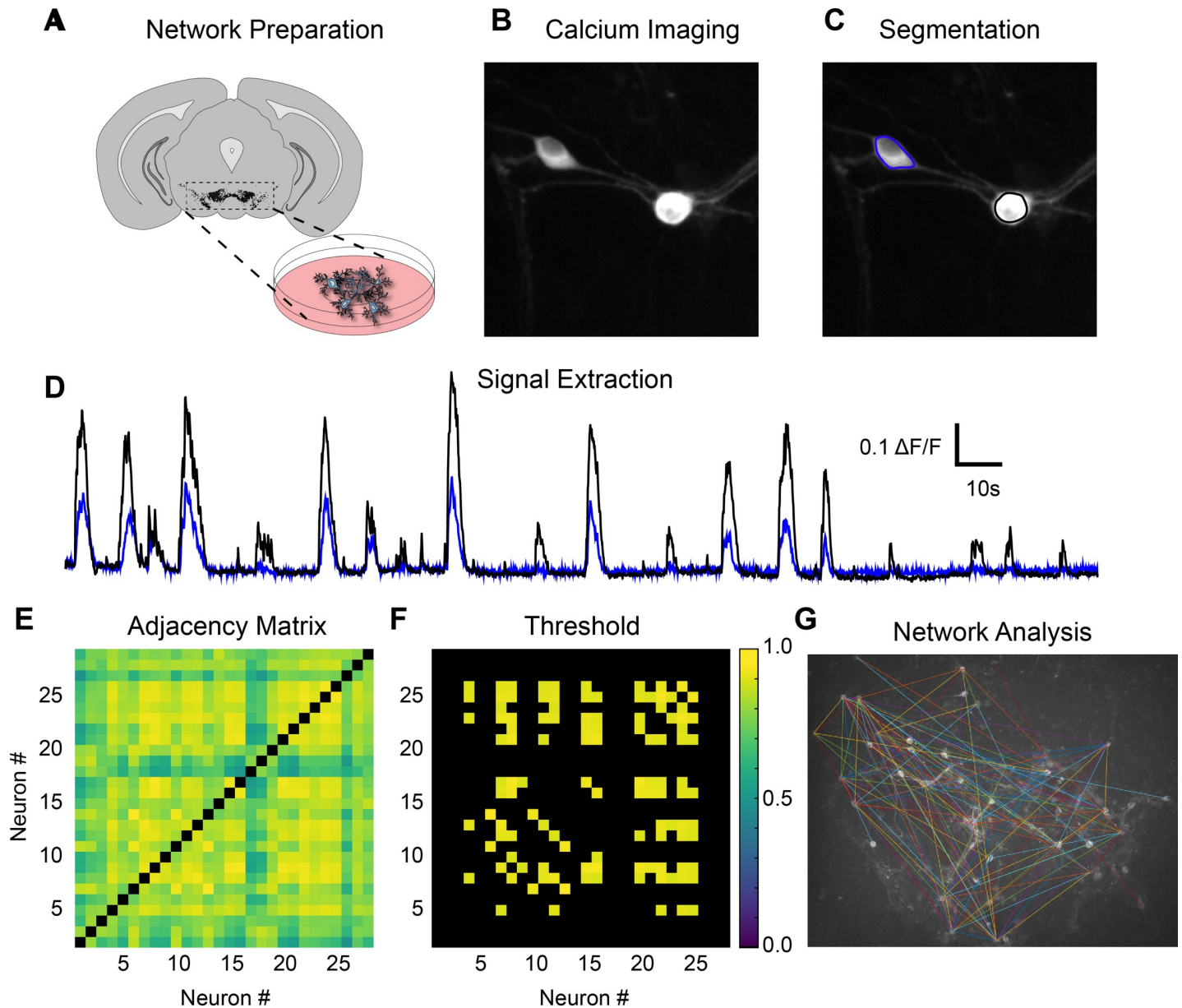
Fig 2. Analysis of functional connectivity in neuronal networks using calcium activity. (A) Midbrain networks cultures are prepared from P0-P1 mice by extraction of the ventral midbrain (dotted box) and viral production of GCaMP6f. (B) Spontaneous calcium activity is monitored in a 10X imaging field at 10 Hz. (C) Neuronal somas are segmented based on visual activity. (D) Time-resolved calcium signals are extracted from each segmented neuron. (E) Spearman's rho correlations between each neuron's activity over the experimental condition are used to create the full functional connectivity matrix. As these matrices represent undirected networks, the graph is symmetrical along the origin (black boxes) with each half of the matrix redundant to the other. (F) A threshold is applied to the matrix to retain a proportion of the fully connected matrix (strongest 15% depicted). (G) Using a 15% proportional threshold, neurons with strong functional connectivity are connected by a line between somas (arbitrary colors). Analyses are performed on 2–4 separate network cultures per day.

https://doi.org/10.1371/journal.pone.0222957.g002

[31]. Furthermore, determining how the network responds to change, either through drug exposure or disease state, our model provides the first step towards understanding how changes in neuron-to-neuron communication underlie more complex responses. It should be noted that the cultured network model is expressly removed from both inputs and outputs that are maintained from a regionally intact system, such as an acute brain slice, and therefore could be used to investigate intrinsic and self-organizing principles that would be reconciled
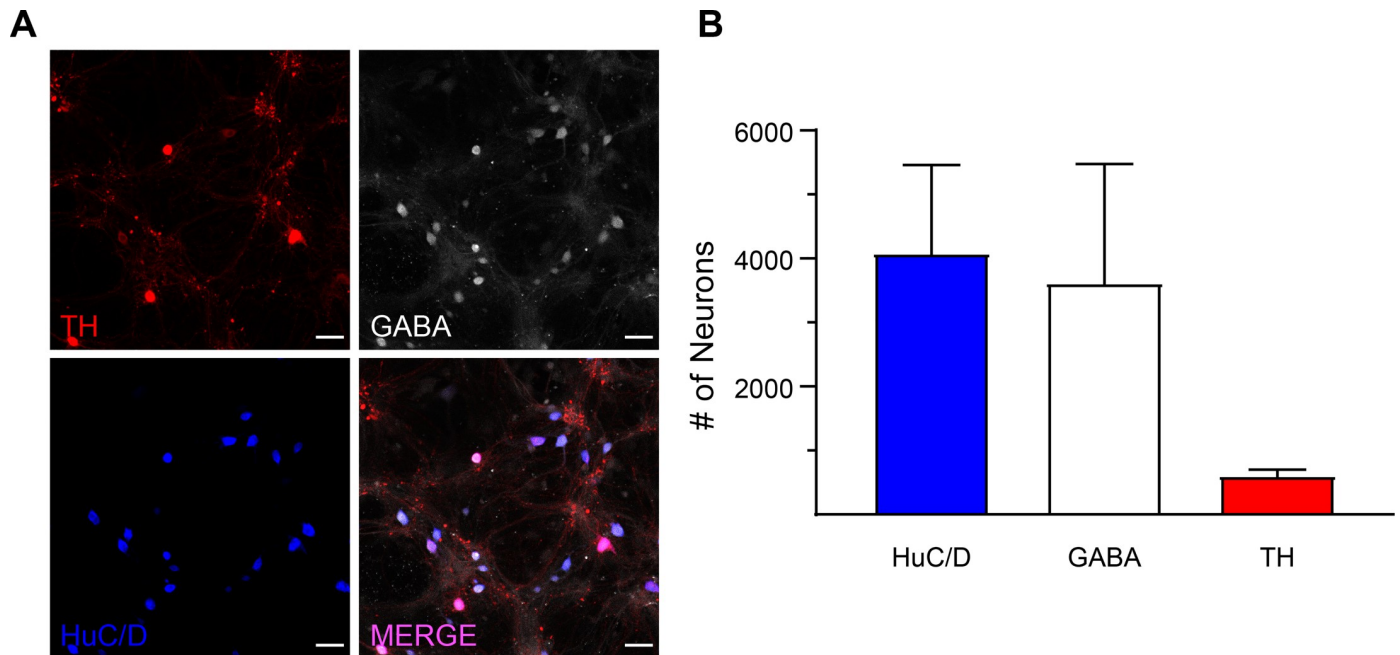
Fig 3. Characterization of neurons in our model system. (A) Neurons are identified immunohistochemically by HuC/D (a general neuronal marker–blue, mean = 4085 ± 1419 from 7 independent replicates), GABA (neurotransmitter product of GAD65 and GAD67 –white, mean = 3619 ± 1900, from 3 independent replicates), or tyrosine hydroxylase (rate-limiting enzyme of dopamine synthesis–red, 609 ± 134, from 6 independent replicates). Scale bar = 40 μm. (B) GABAergic neurons are the predominant neuronal type in ventral midbrain neuronal culture. Data are presented as mean ± SD.

https://doi.org/10.1371/journal.pone.0222957.g003

in model system receiving multiple overlapping inputs. Future experiments will be necessary to elucidate differences between ventral midbrain network cultures and midbrain slice preparations.

Methamphetamine suppression of network activity is D$_2$ receptor dependent

Increases in action potential frequency have been shown to correlate with increased amplitude and duration of GCaMP6f fluorescence signal [32]. As such, integration of fluorescence signals is commonly used to estimate neuronal activity [33–35]. To determine whether methamphetamine differentially affects the activity of individual neurons as well as the overall network output, the spontaneous calcium signals at baseline were integrated and plotted against the spontaneous calcium signals during methamphetamine treatment. Comparing the neuronal activity of each neuron before and during methamphetamine treatment, we found during methamphetamine exposure, the activity of all neurons skews below unity, suggesting methamphetamine decreases the overall activity of the network (Fig 5B and 5C) (One-way ANOVA *$p < 0.05$, **$p < 0.01$, ****$p < 0.0001$, $F_{(2, 307)} = 14.03$; n = 71–125 neurons from 3–4 coverslips per group; mean ± SD). These data are consistent with the hypothesis that methamphetamine not only decreases activity of individual GABA neurons but also manifests across the network. We reasoned that methamphetamine induces network suppression, theoretically, through modification of synaptic signaling.

Methamphetamine has been shown to increase extracellular dopamine levels via two different mechanisms: increased firing activity of dopamine neurons and via the dopamine transporter-mediated dopamine efflux–the action potential-independent mechanism of dopamine release [22,29,36]. The released dopamine binds to dopamine receptors on the neighboring
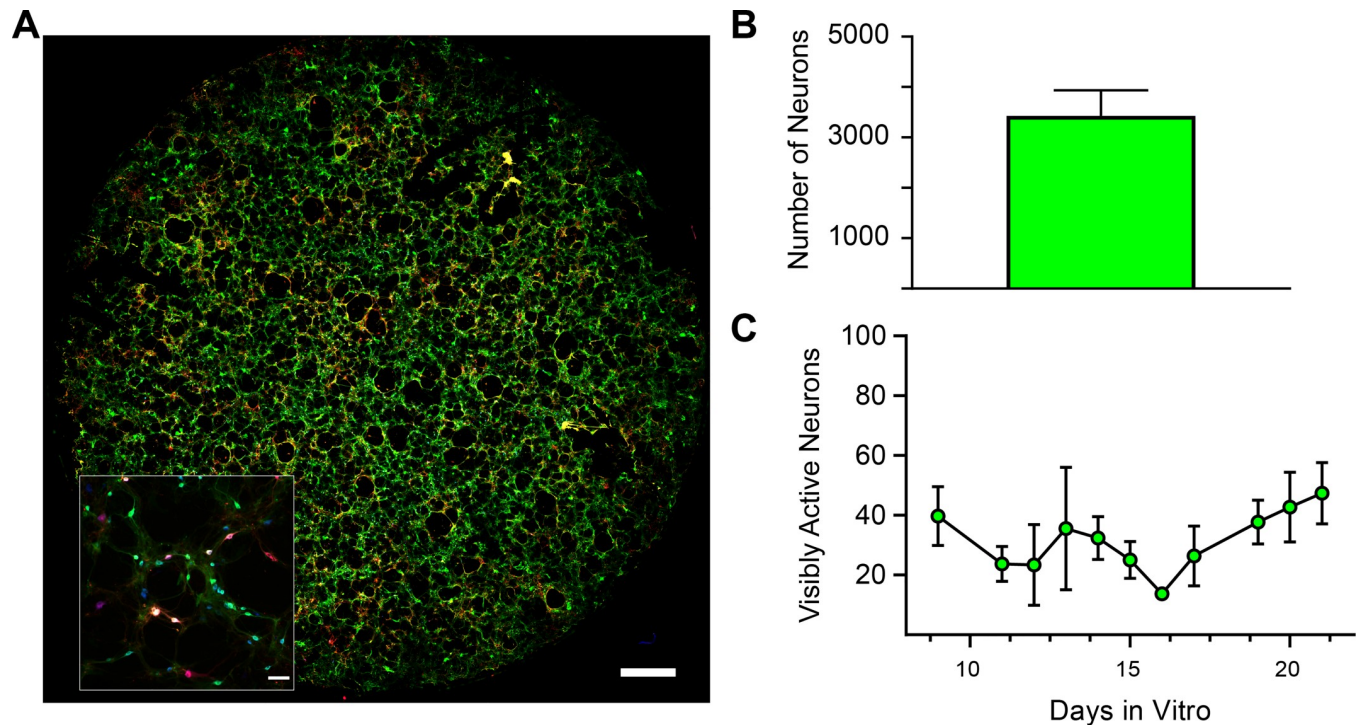
Fig 4. Length of neuronal culture does not affect number of neurons in our model system. (A) Representative image of ventral midbrain neurons. Scale bar = 1000 μm. Inset shows neurons from representative image stained for GCaMP6f (green), tyrosine hydroxylase (red), HuC/D (blue). Inset scale bar = 75 μm. (B) Coverslips are comprised of approximately 3400 neurons. Data are presented as mean ± SD. (C) No significant change in visibly active neurons across all days (simple linear regression, p = 0.0916, r^2 = 0.08383; mean ± SD, from 3 independent replicates per day).

neurons to modulate their activity [4,5]. D_2 receptors are negatively coupled to adenylyl cyclase, and agonist activation of D_2 receptors decreases neuronal activity [37]. The ventral midbrain GABAergic neurons [16], which are the principal neuronal type in our model system, express D_2 receptors [7]. Therefore, methamphetamine-stimulation of dopamine release is predicted to activate D_2 receptors on these GABAergic neurons, leading to network suppression. Thus, we hypothesized that methamphetamine suppression of ventral midbrain neuronal network activity is mediated through a D_2 receptor-dependent mechanism. We tested this hypothesis by examining ventral midbrain neuronal network activity in the presence or absence of D_2 receptor blockade (sulpiride, 5 μM), before and during methamphetamine treatment. Our analysis revealed that blockade of D_2 receptor inhibited the methamphetamine suppression of neuronal network activity (Fig 5C). Importantly, we found that sulpiride blockade of D_2 receptors not only inhibited methamphetamine suppression of network activity but also increased network activity above baseline (n = 71 to 134 neurons, from 6 independent replicates, one-way ANOVA with Tukey's post-hoc multiple comparisons, p < 0.05, F (2, 307) = 14.03. All comparisons performed at DIV 11.). These data are consistent with the interpretation that methamphetamine-induced suppression of network activity is D_2 receptor dependent, and ventral midbrain cultured neuronal networks are under inhibitory regulation of D_2 receptor at baseline. Dopaminergic terminals contact adjacent and distal GABAergic cells [38,39]. These contacts provide the structural basis for dopamine modulation of individual synapses locally and the interconnection distal networks at baseline under physiological conditions. It should be noted that at the cellular level, the intrinsic excitability and synaptic efficacy of a single neuron is always under concomitant modulation of multiple neuromodulators.
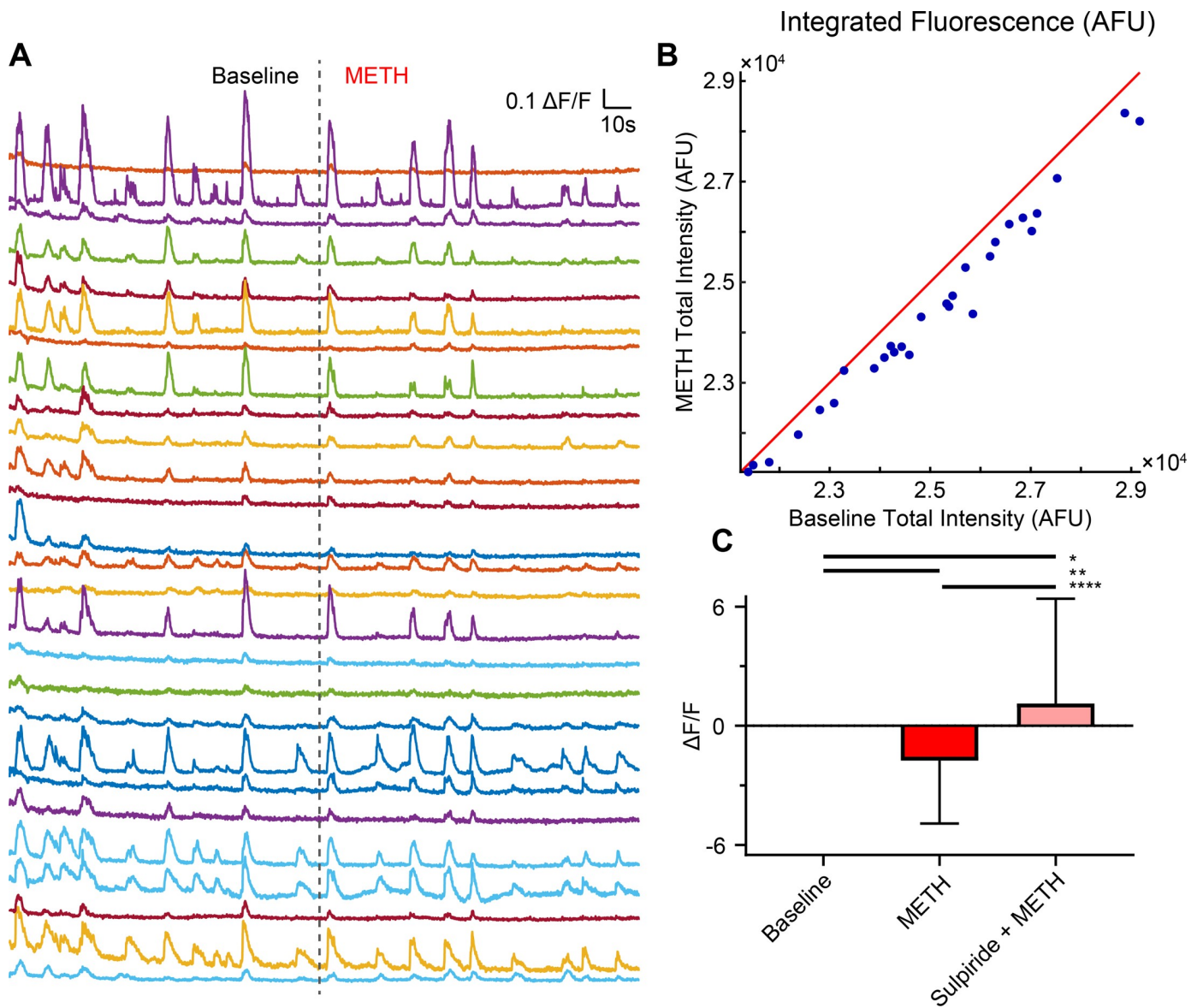
Fig 5. Methamphetamine exposure decreases midbrain neuronal activity via a D_2 receptor mechanism. (A) Calcium activity of neurons is monitored at baseline and during methamphetamine addition (dotted line). (B) Scatter plot of the total intensity per neuron (blue dots) showing activity skewing below unity (red line) to the baseline condition, indicating activity is suppressed. (C) Methamphetamine-induced increases in dopamine may suppress the activity of GABAergic neurons through D_2 receptor activation. Methamphetamine-induced suppression of integrated fluorescence analysis is blocked by D_2 receptor antagonism (sulpiride, 5 μM) leading to increased network activity (One-way ANOVA $^*p < 0.05$, $^{**}p<0.01$, $^{****}p<0.0001$, $F(2, 307) = 14.03$; n = 3–4 independent replicates per experimental group; mean ± SD).

https://doi.org/10.1371/journal.pone.0222957.g005

Therefore, reconfiguration of neural network by neuromodulators is an intricately balanced process that involves multiple synergistic or antagonistic pathways. The current study does not address these complex interactions. Bridging multiple levels of analyses including the activity of single neuron, local and distant networks can address these possibilities.

Methamphetamine does not modify changes in ventral midbrain neuronal network functional connectivity but alters topological structure

So far, our data suggest that methamphetamine suppresses ventral midbrain cultured neuronal network activity. However, it remains unknown whether methamphetamine modulates

functional connectivity. Furthermore, the relationship between development and functional connectivity in ventral midbrain neuronal networks has not been studied. Previous reports investigating hippocampal and cortical neural networks have shown that functional connectivity increases across development [12,14]. Therefore, we investigated whether the functional connectivity of ventral midbrain neuronal networks is also altered by development and if methamphetamine modulates this potential development-dependent regulation of ventral midbrain neuronal networks. We found, in the absence of drug treatment (baseline), that there is a significant decrease in the functional connectivity across network development with an average of 0.71 at DIV 9 (DIV: Days *In Vitro*) to 0.54 on DIV 21 with a decay of 0.02 per day (simple linear regression, $p < 0.01$, $r^2 = 0.2098$, n = 3 independent experiments per DIV) (Fig 6A, black). These data are specifically important because the total number of neurons, the number of active GCaMP6f neurons, and thus network size, did not change across days (Fig 4C). Therefore, the age-dependent decreases in the functional connectivity suggest a developmentally related (fine tuning) maturation or elimination of the network. However, since networks were of similar size, it is not clear whether this observed phenomenon is dependent on the total number of neurons observed within the network.

During methamphetamine exposure, similar decreases in functional connectivity of the network across development were observed with an average of 0.65 at DIV 9 and 0.40 at DIV 21 with a decay 0.014 per day (simple linear regression, $p < 0.05$, $r^2 = 0.1394$, n = 3 independent experiments per DIV) (Fig 6A, red). This suggests that the observed changes in functional connectivity are robust against acute methamphetamine exposure. Though methamphetamine exposure has previously been shown to exert pathological effects [40,41], these were not observed to directly manifest at the level of average connectivity. These data suggest methamphetamine did not alter average functional connectivity across developmental days studied here; therefore, we hypothesized that methamphetamine had unevenly altered a subset of connections–for example, strong connections get stronger while weak connections get weaker– that may be obfuscated by average measurements. To address this hypothesis, we generated a connection value density plot during baseline and during methamphetamine treatment (Fig 6B). Connectivity was observed to be predominantly positive in baseline and during methamphetamine exposure. However, the distribution around the unity line appeared to be uneven, with highly connected neuronal pairs from baseline dropping out and becoming negatively connected in response to methamphetamine. To evaluate this, a histogram was generated to evaluate the distance from the unity line for each neuronal pair (Fig 6C). The magnitude of the measurement quantifies the strength of change between condition with positive values, indicating large changes in favor of the methamphetamine condition and negative values favoring the baseline condition. The distribution was found to show non-normal distribution (Kolmogorov-Smirnov, $p < 0.05$, n = 20,216 pairwise connections, from 35 independent experiments) with a significant, but modest, positive mean value (Wilcoxon signed rank, $p < 0.01$, n = 20,216 pairwise connections, from 35 independent experiments). From the histogram, negative skewing was readily apparent (skewness = -0.5417, n = 20,216 pairwise connections, from 35 independent experiments) and further kurtosis testing, a tail-distribution metric, revealed stronger than normal contribution (kurtosis = 6.3653, normal distribution kurtosis = 0, n = 20,216 pairwise connections, from 35 independent experiments). This finding reveals that a significant subset of connections dropout during methamphetamine exposure. As the network is predominantly GABAergic (~88% Fig 3B), this suggests that non-GABAergic neurons are most likely to be those that dropout. This implies that changes in connectivity are particularly nuanced. Future studies will be necessary to identify the specific neuronal phenotypes implicated in these changing connections, whether they be dopaminergic-dopaminergic, GABAergic-dopaminergic, or GABAergic-GABAergic connections.
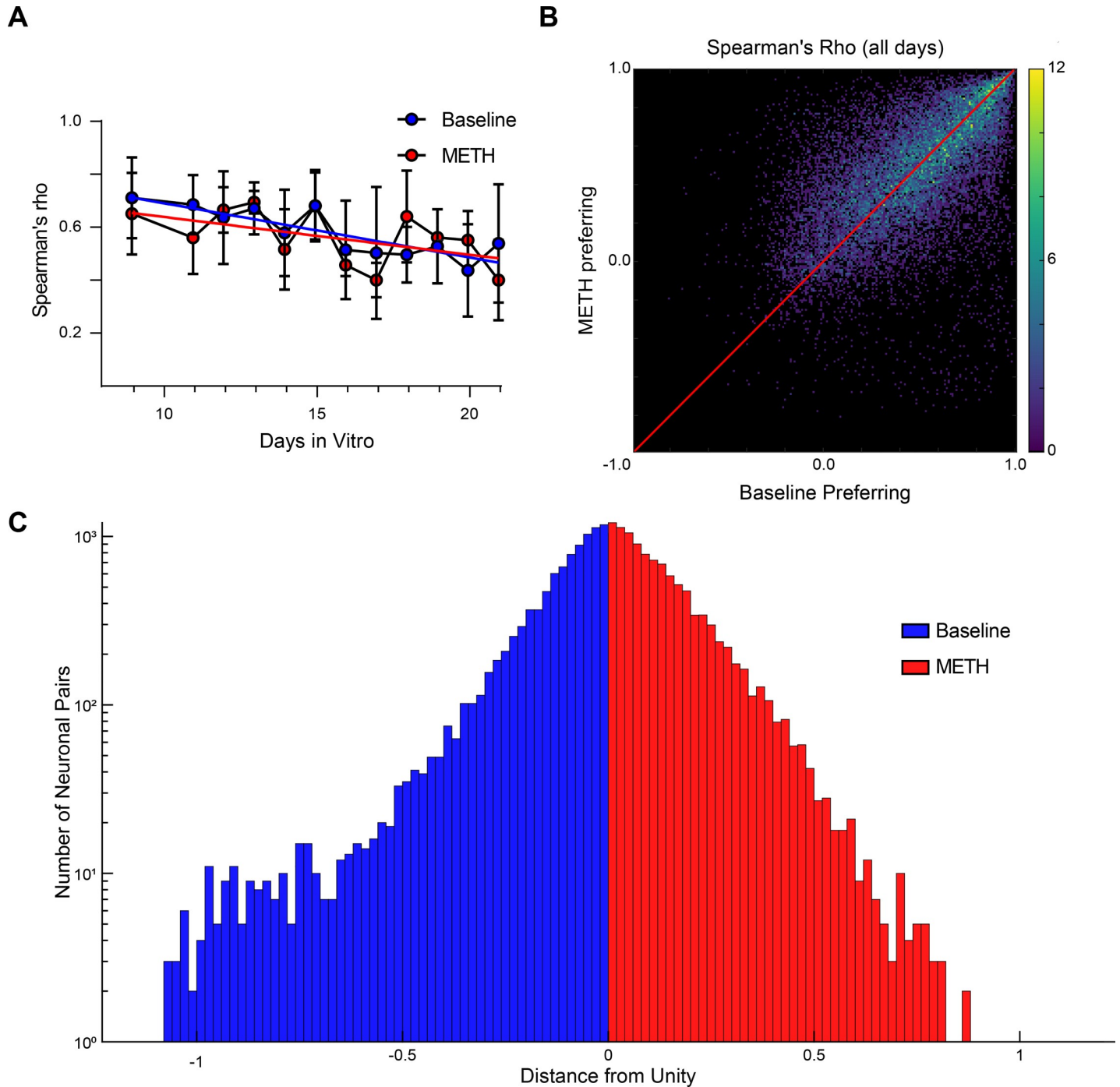
Fig 6. Time-dependent decay of functional connectivity is not affected by methamphetamine exposure. (A) Despite being highly active, functional connectivity of neuronal networks decayed significantly with network age and persisted in the presence of methamphetamine (simple linear regression; baseline p < 0.01, METH p < 0.05; n = 3 independent experiments per DIV; mean ± SD). (B) Three-dimensional histogram of functional connectivity in baseline versus methamphetamine between all neurons across all days reveals an asymmetric distribution around unity (red line) skewing towards baseline. (n = 20,216 pairwise connections, from 35 independent experiments). (C) Deviations from unity were compared between baseline-favoring (below unity) pairwise neuronal correlations and methamphetamine-favoring (above unity) pairwise neuronal correlations.

https://doi.org/10.1371/journal.pone.0222957.g006

The absence of change(s) in the functional connectivity may or may not coincide with change(s) in the network structure. Therefore, we sought to identify and quantify the

methamphetamine-modulation of ventral midbrain neuronal network topology. We applied a commonly used 15% proportional threshold [42–44] to isolate the strongest 15th percentile of connections before and during methamphetamine exposure. This analytical approach revealed a qualitative rearrangement of a connectivity in the strongest connections (Fig 7A and 7B). These data are consistent with the hypothesis that topological features of a methamphetamine treated network diverge from their drug-naïve counterpart. In order to further investigate this hypothesis, we applied a weighted assortativity measure and found that assortativity significantly increased across development. While both baseline and methamphetamine conditions increased across days in culture (Two-factor ANOVA $p < 0.01$, $F_{(11, 46)} = 3.669$, 38.51% of total variation, n = 3 independent experiments per DIV), only the methamphetamine condition reached significance criteria (simple linear regression, $p < 0.01$, $r^2 = 0.2218$, n = 3 independent experiments per DIV) (Fig 7C). The observed increase in assortativity ranged from negative assortativity on DIV11 that converted to positive assortativity starting at DIV14, continually increasing up to DIV21. These data suggest that, as observed in previous studies, communication in younger cultured networks is more vulnerable to neuronal loss during methamphetamine exposure, while that in older cultured networks are more resilient. However, it is not directly clear why the network drastically reorganized in the early culture age and, specifically at which level this is directly modulated across culture age. In addition, network maturation may provide a compensatory refinement of connections that favors positive assortativity and reduces the impact of methamphetamine-induced toxicity [45–48]. Future experiments may reveal whether there are changes in molecular expression patterns, receptor interactions, or structural connectivity changes that may underlie this observation.

In addition, we analyzed other common metrics in network analysis such as network clustering or modularity. Clustering coefficient determines the interconnectedness, whereas, modularity index is an efficiency metric describing how well the clusters are classified into subnetworks. We found that neither development nor acute methamphetamine exposure affected network clustering or modularity (Fig 7D and 7E) (two-way ANOVA with Sidak's multiple comparisons test, $p > 0.05$, $F_{(11, 46)} = 0.3424$ clustering, $F_{(11, 46)} = 0.7777$ modularity, n = 3 independent experiments per DIV). Though non-significant, there may be apparent trends, e.g. trend-wise increases in modularity across both conditions and initial decreases in clustering that were negligible in aged cultures, that were not uncoverable in our sample sizes or range of culture age. In addition, we also analyzed the D_2 receptor dependencies for network clustering, modularity and assortativity metrics but did not observe any significant effects on these measures (S1 Fig, $p > 0.05$, $F_{(2, 7)} = 1.767$ clustering, $F_{(2, 7)} = 0.08639$ modularity, $F_{(2, 7)} = 1.601$ assortativity, n = 3–4 independent experiments per group. All comparisons performed at DIV 11). These data are consistent with the interpretation that methamphetamine exposure alters cultured network assortativity independent of D_2 receptor activity. While these results were unexpected, they illustrate that the effects of methamphetamine scale from neurons to the network. Furthermore, the D_2 receptor activity was not found to be responsible for changes in network structure and function. Rather, methamphetamine exposure leads to perturbations in multiple modalities, such as receptors, intrinsic neuronal properties, and neuroimmunological factors, that may scale to the network topology.

The major findings in terms of network reorganization in this study were a loss of neuron pairs in response to methamphetamine (Fig 6) and the demonstration that younger cultures are more vulnerable to neuronal loss during methamphetamine exposure, resulting in dramatic reorganization. These effects can be explained through "symmetry breaking" in a network. Broadly, in a symmetric network, each neuron is, at the least, reciprocally connected to each other. The extreme condition is where each neuron is connected to every other neuron. In this example, should one cluster of neurons become active, it quickly propagates and
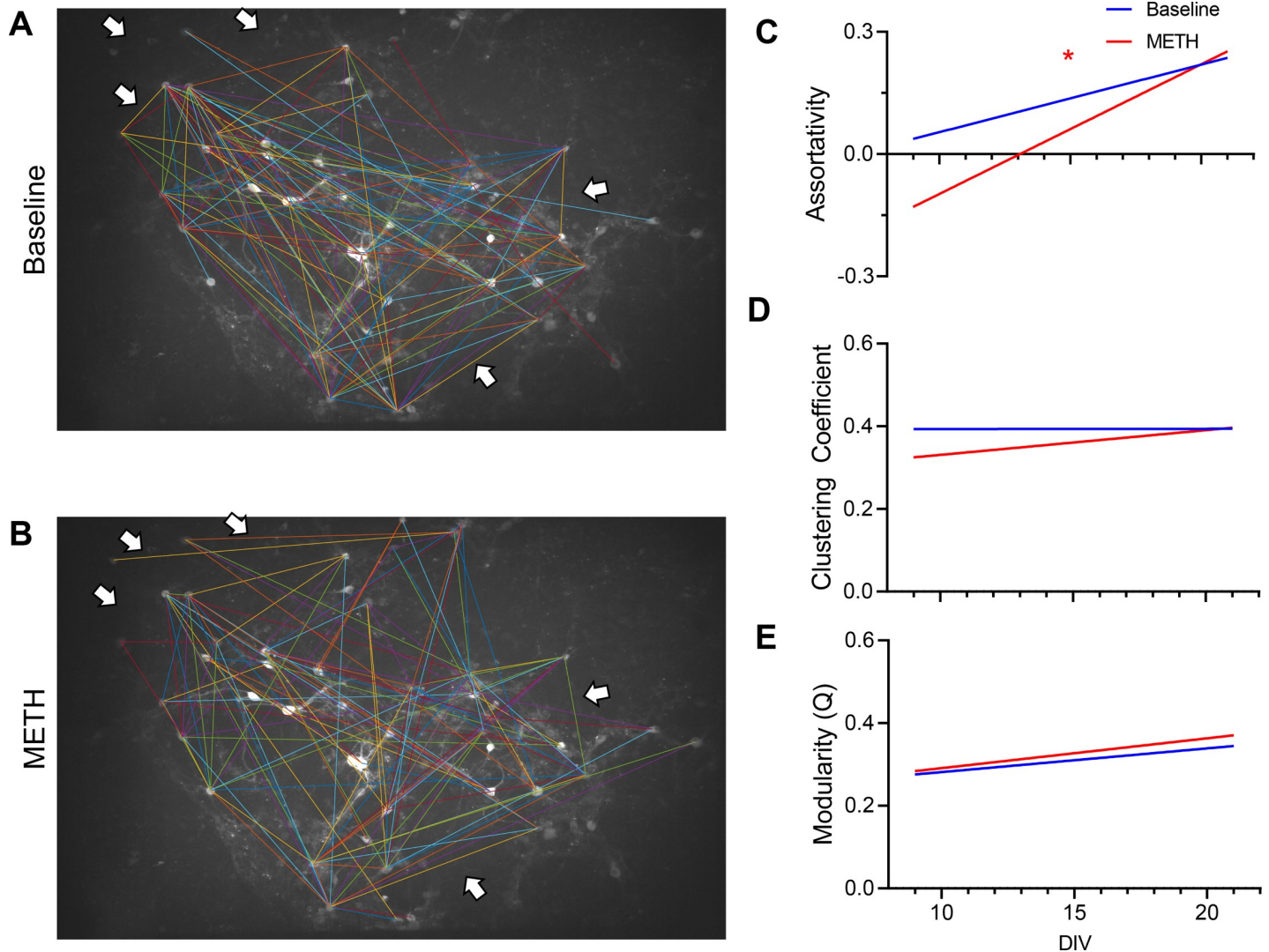
Fig 7. Methamphetamine and age of cultured network modulate functional network topology. (A,B) To minimize differences in network size, 15% proportional thresholds were applied during baseline (A) and in the presence of methamphetamine (B) to emphasize connection gains/losses (white arrows). (C) Network assortativity increases significantly across days (Two-factor ANOVA p < 0.01, F (11, 46) = 3.669, 38.51% of total variation, n = 3 independent experiments per DIV) but not between baseline and methamphetamine (p = 0.1078, F (1, 46) = 2.690, 2.566% of total variation, n = 3 independent experiments per DIV). No significant interaction was observed between DIV and condition (p = 0.1750, F (11, 46) = 1.472, 15.45% of total variation, n = 3 independent experiments per DIV). While increases across DIV at both baseline and in the presence of methamphetamine, only methamphetamine reached statistical significance (linear regression, p < 0.01, r^2 = 0.2218 METH, p = 0.0988 r^2 = 0.08042 Baseline, n = 3 independent experiments per DIV). Data presented as lines of best fit from simple linear regression. (D, E) To investigate interconnectivity and community restructuring, clustering coefficients and modularity index (Q) were calculated across DIV and conditions, but no significant trends or effects were observed. Data presented as lines of best fit from simple linear regression.

https://doi.org/10.1371/journal.pone.0222957.g007

disperses. However, symmetric breaking, which can occur through pruning, enhancement of synapses, etc., provides the mechanism by which undirected activity propagation in the symmetric network can become directed and rhythmic [49,50]. Activity has a favored direction of flow which is reinforced every time a pathway is taken, further enhancing the asymmetry. Therefore, the vulnerability of younger networks to methamphetamine exposure potentially speaks to a lack of symmetry breaking in the network. Simply, not enough time has passed to favor certain connected pathways over others. Similarly, the dropping out of neurons during methamphetamine exposure suggests that the network converges on a minority of potential

asymmetric pathways. Simply stated, methamphetamine reduces the repertoire of potential pathways that the activity can move, providing a network-level description on the neurobiological basis of addiction.

The work presented here represents the first foray, to our knowledge, in determining the mechanisms of ventral midbrain network modulation by methamphetamine. Ventral midbrain networks were found to exhibit development-specific changes in functional connectivity and topological changes during methamphetamine exposure. While this study attempted to isolate D_2 receptor-dependent differences, further studies are warranted to determine interaction effects between multiple receptor types and subtypes. Systematic blockade of receptors may provide clues into the polypharmacy necessary to reverse the effects of methamphetamine exposure that are not readily observable using previously established methodologies.

Establishing this methodology provides a unique framework to explore ventral midbrain networks across multiple modalities. For example, using dopaminergic enrichment methods [51] permits the evaluation of dopaminergic contributions to network structure and function. These can be coincided with simultaneous imaging of stress indicators and network electrophysiology when grown on microelectrode arrays to provide both high temporal resolution of neuronal activity and correlative changes in neuronal stress.

This study examined the effects of acute methamphetamine exposure, and further studies can utilize repeated exposure paradigms across development, thereby not only tracking network evolution but also whether and how methamphetamine exposure modifies this. Previous studies investigating networks enriched in dopaminergic content [42,43,52] have focused on whole-brain interactions that do not uncover differences at the single-neuron resolution. Differences at the single-neuron resolution may compound upon repeated exposures and yield progressive transitions across the network that precede the onset and underly the establishment of untoward consequences of methamphetamine exposure. Ultimately, this study provides the fundamental basis for the continued exploration of ventral midbrain network modulation and diseases associated with dopaminergic dysfunction.

Materials and methods

Animals

Wild-type (WT) C557BL/6J male and female mice were obtained from The Jackson Laboratory (Bar Harbor, Maine). All animals were maintained in the University of Florida animal facilities. All experiments were approved by the Institutional Animal Care and Use Committee at University of Florida.

Primary ventral midbrain culture

Full protocol for preparation is available at: https://www.protocols.io/private/C16AFE64BBD5 72063A78466BB79CCDDD

Briefly, dissociated post-natal ventral midbrain cells from C57BL6/J mice of either sex comprising neurons and glia were plated at 80,000 cells per coverslip. Ventral midbrain cultures were grown in 2 mL Neurobasal Plus supplemented with B-27 plus, 2 mM L-glutamine, 1 ng/mL GDNF, 0.4 mM kynurenic acid. Media was exchanged every 4 days by removing 1 mL old media and adding 1 mL fresh media (without GDNF/kynurenic acid supplement).

Viral transduction

Cultures prepared from C57BL6/J mice were transduced with AAV5.Syn.GCaMP6f.WPRE. SV40 (MOI: 30,000) on DIV 0. AAV5.Syn.GCaMP6f.WPRE.SV40 was a gift from The

Table 1. Composition of ACSF.

ACSF (pH 7.4, 310 mOsm)			
Chemical	Concentration	Vendor	Catalog Number
NaCl	126 mM	Sigma-Aldrich	S7653-1KG
KCl	2.5 mM	Sigma-Aldrich	P9541-500G
CaCl2	2 mM	Sigma-Aldrich	223506-500G
NaH2PO4	1.25 mM	Sigma-Aldrich	71505-250G
MgSO4	2 mM	Sigma-Aldrich	M7506-500G
Dextrose	10 mM	Sigma-Aldrich	D9434-500G

Genetically Encoded Neuronal Indicator and Effector Project (GENIE) & Douglas Kim (Addgene viral prep # 26973-AAV5). Neurons were imaged after sufficient expression was observed between DIV 9 and DIV 21.

Calcium imaging

Briefly, mouse midbrain networks were transferred to the recording chamber and imaged under constant gravity perfusion of artificial cerebral spinal fluid (ACSF, Table 1) at 37C. A Spectra X equipped with 7 excitation lines configured with a Mightex Polygon400 Digital Micromirror Device was used to excite both GCaMP6f (λ_{ex} = 470 nm) through a quad-pass filter (Chroma Technologies, Brattleboro, Vermont), Nikon CFI Plan Fluor 10XW objective (NA = 0.3) and detected with an Andor Zyla 4.2 sCMOS 12-bit camera at 10 frames per second. Videos were acquired with a 2-minute baseline of spontaneous network activity in ACSF and a 2-minute experimental condition in ACSF, ACSF with 10 μM methamphetamine, or 10 μM methamphetamine and 5 μM sulpiride.

Image processing

Videos were imported into ImageJ2 via the Bio-Formats Importer plugin and converted into 8-bit TIFF stacks. Image drift was corrected using the moco plugin when necessary [53]. Regions of interest (ROI) for neuronal cell bodies were segmented manually and signals were exported into CSV files. Only visibly spontaneous active neurons with non-overlapping, distinguishable somas were segmented.

Functional connectivity and quantification of network topology

CSV files were imported into MATLAB (Mathworks Cambridge, MA). Calcium signals were normalized and expressed as $F(t) = \Delta F/F_0$ where F_0 is defined as the baseline condition. Pairwise Spearman's correlation coefficients were determined over the entire 2-minute time series of each condition between neurons (MATLAB function: corr, type: Spearman). Densiometric measures were applied using a range of thresholds ranging from correlation values of 0.05 to 1 with 0.05 step-size and averaged by day and condition. To quantify changes in network topology of the strongest connections, a 15% proportional threshold retaining the 15% strongest connections were applied to each adjacency matrix. Applying thresholds also improved the ability to compare across networks that varied in size. Network clustering assortativity, clustering coefficient, and modularity were calculated using the Brain Connectivity Toolbox [9]. All calculations retained weighted values, and undirected weighted versions of the respective metrics were used where appropriate [54–56]. Importantly, these metrics are performed on activity networks with single-cell resolution and are not assumed to reflect synaptic connectivity. Furthermore, sampling rates were appropriate to investigate functional but not effective

connectivity in these networks and are outside the scope of the current investigation. Future studies should investigate the synaptic and effective connectivity differences across ventral midbrain networks.

Immunocytochemistry and network characterization

Immunocytochemistry–Cultures were washed three times in phosphate buffered saline (PBS), fixed in 4% paraformaldehyde in PBS, and washed three more times in PBS. Cultures were then blocked and permeabilized in 0.5% Triton X-100 and 10% normal goat serum (NGS) for 30 minutes at room temperature, followed by three washes in PBS. Cultures were incubated overnight in primary antibody solution containing mouse anti-TH (1:500), mouse anti-HuC/D (1:500), and rabbit anti-GFP (1:500) or rabbit anti-GABA (1:1000). Negative controls utilized antibody dilution solution without primary antibodies. Cultures were then washed three times for 20 minutes at room temperature on an orbital shaker. Then cultures were incubated in secondary antibody solution containing Goat Anti-Rabbit Alexa Fluor 488 conjugated, Goat Anti-Mouse IgG1 Alexa Fluor 568 conjugated, and Goat Anti-Mouse IgG2b Alexa Fluor 647 or Goat Anti-Rabbit Alexa Fluor 405 conjugated antibodies on an orbital shaker in the dark for one hour at room temperature. All antibodies were diluted with 5% normal goat serum in 0.1% Triton X-100 in PBS. Cultures were then washed three times for 20 minutes at room temperature on an orbital shaker in the dark. Finally, cultures were mounted on slides using either Fluoromount-G or DAPI Fluoromount-G and allowed to harden. Reagent catalog numbers are presented in Table 2.

Imaging and Quantification–Coverslips were imaged in their entirety utilizing a Keyence BZ-X700 microscope with the stitching module through a Nikon CFI Plan Apo λ 10X objective, metal halide lamp, and Keyence standard filters for each channel. Stitched images of each channel were exported as single-channel TIFF images. TIFFs were imported into ImageJ2. Neuronal cell bodies were identified by HuC/D and or DAPI signal. GCaMP6f expressing cells were identified by GFP signal. Dopaminergic neurons were identified by TH signal. GABAergic neurons were identified by GABA signal. All neurons were counted manually.

Table 2. Immunocytochemistry reagents utilized in this study.

Chemical	Concentration	Vendor	Catalog Number
Phosphate Buffered Saline	N/A	N/A	N/A
Triton X-100	Varies	Fisher	BP151-100
Normal Goat Serum	Varies	Lampire Biological Products	7332500
Rabbit Anti-GABA	1:1000	Immunostar	20094
Rabbit Anti-GFP	1:500	Invitrogen	A-11122
Mouse Anti-Tyrosine Hydroxylase	1:500	Sigma-Aldrich	T1299
Mouse Anti-HuC/D	1:500	Invitrogen	A-21271
DAPI Fluoromount-G	N/A	Southern Biotech	0100–20
Fluoromount-G	N/A	Southern Biotech	0100–01
Paraformaldehyde	4%	Electron Microscopy Sciences	15714-S
Goat Anti-Rabbit IgG (H+L) Alexa Fluor 405	1:500	Invitrogen	A-31556
Goat Anti-Mouse IgG1 Alexa Fluor 568	1:500	Invitrogen	A-21124
Goat Anti-Mouse IgG2b Alexa Flour 647	1:500	Invitrogen	A-21242
Goat Anti-Rabbit IgG (H+L) Alexa Fluor 488	1:500	Invitrogen	A-11034

Statistical analysis

All statistical analysis was performed in Graphpad Prism version 8.02 for Windows, GraphPad Software, La Jolla, California, USA. Linear regression, one-way ANOVA, and two-way ANOVA were used where appropriate and corrected for multiple comparisons using either Tukey's or Sidak's post-hoc test. Effects were considered significant at α = 0.05. Data are presented with mean and standard deviation unless otherwise stated.

Supporting information

S1 Fig. Specific network topology modification by methamphetamine is not D2 receptor dependent. (A) To assess whether D_2 receptor availability alters network function, similar age networks were exposed to either continued baseline or methamphetamine in the presence of sulpiride. Neither methamphetamine exposure nor sulpiride co-administration produced a significant change (One-way ANOVA, p = 0.2677, F (2, 7) = 1.601; mean ± SD). (B,C) Network clustering and modularity are unaltered by either exposure to methamphetamine alone or with co-administration of sulpiride (One-way ANOVA, p = 0.2392, F (2, 7) = 1.767, clustering coefficient; p = 0.9182, F (2, 7) = 0.08639, modularity; mean ± SD). Data are presented as mean relative change ± SD.
(TIF)

Acknowledgments

We thank Jack Kennedy for valuable input in data analysis.

Author Contributions

Conceptualization: Douglas R. Miller, Andrew P. Maurer, Habibeh Khoshbouei.

Data curation: Douglas R. Miller, Dylan T. Guenther.

Formal analysis: Douglas R. Miller, Alexander J. Refowich, Carissa Hansen, Andrew P. Maurer.

Funding acquisition: Andrew P. Maurer, Habibeh Khoshbouei.

Investigation: Douglas R. Miller, Joseph J. Lebowitz.

Methodology: Douglas R. Miller, Andrew P. Maurer, Habibeh Khoshbouei.

Project administration: Andrew P. Maurer, Habibeh Khoshbouei.

Resources: Andrew P. Maurer, Habibeh Khoshbouei.

Software: Douglas R. Miller, Dylan T. Guenther.

Supervision: Andrew P. Maurer, Habibeh Khoshbouei.

Validation: Douglas R. Miller, Joseph J. Lebowitz.

Visualization: Douglas R. Miller, Dylan T. Guenther, Andrew P. Maurer, Habibeh Khoshbouei.

Writing – original draft: Douglas R. Miller.

Writing – review & editing: Douglas R. Miller, Andrew P. Maurer, Habibeh Khoshbouei.

References

1. Di Chiara G, Imperato A. Drugs abused by humans preferentially increase synaptic dopamine concentrations in the mesolimbic system of freely moving rats. Proc Natl Acad Sci U S A 1988; 85:5274–8. https://doi.org/10.1073/pnas.85.14.5274 PMID: 2899326

2. Rice ME. Distinct regional differences in dopamine-mediated volume transmission. Prog. Brain Res., vol. 125, Elsevier; 2000, p. 277–90. https://doi.org/10.1016/S0079-6123(00)25017-6 PMID: 11098664

3. O'Neill B, Patel JC, Rice ME. Characterization of Optically and Electrically Evoked Dopamine Release in Striatal Slices from Digenic Knock-in Mice with DAT-Driven Expression of Channelrhodopsin. ACS Chem Neurosci 2017; 8:310–9. https://doi.org/10.1021/acschemneuro.6b00300 PMID: 28177213

4. Beckstead MJ, Grandy DK, Wickman K, Williams JT. Vesicular dopamine release elicits an inhibitory postsynaptic current in midbrain dopamine neurons. Neuron 2004; 42:939–46. https://doi.org/10.1016/j.neuron.2004.05.019 PMID: 15207238

5. Branch SY, Beckstead MJ. Methamphetamine produces bidirectional, concentration-dependent effects on dopamine neuron excitability and dopamine-mediated synaptic currents. J Neurophysiol 2012; 108:802–9. https://doi.org/10.1152/jn.00094.2012 PMID: 22592307

6. Jiao D, Liu Y, Li X, Liu J, Zhao M. The role of the GABA system in amphetamine-type stimulant use disorders. Front Cell Neurosci 2015; 9:162. https://doi.org/10.3389/fncel.2015.00162 PMID: 25999814

7. Morales M, Margolis EB. Ventral tegmental area: cellular heterogeneity, connectivity and behaviour. Nat Rev Neurosci 2017; 18:73–85. https://doi.org/10.1038/nrn.2016.165 PMID: 28053327

8. Newman MEJ. The Structure and Function of Complex Networks. SIAM Rev 2003; 45:167–256. Pii S0036144503424804\rDoi https://doi.org/10.1137/S003614450342480

9. Rubinov M, Sporns O. Complex network measures of brain connectivity: Uses and interpretations. Neuroimage 2010; 52:1059–69. https://doi.org/10.1016/j.neuroimage.2009.10.003 PMID: 19819337

10. Newman MEJ. Mixing patterns in networks. Phys Rev E 2003; 67:026126. https://doi.org/10.1103/PhysRevE.67.026126 PMID: 12636767

11. Aertsen AMHJ, Gerstein GL, Habib MK, Palm G. Dynamics of Neuronal Firing Correlation: Modulation of "Effective Connectivity" vol. 61. 1989.

12. Teller S, Granell C, De Domenico M, Soriano J, Gómez S, Arenas A. Emergence of Assortative Mixing between Clusters of Cultured Neurons. PLoS Comput Biol 2014; 10:e1003796. https://doi.org/10.1371/journal.pcbi.1003796 PMID: 25188377

13. Bettencourt LMA, Stephens GJ, Ham MI, Gross GW. Functional structure of cortical neuronal networks grown in vitro. Phys Rev E—Stat Nonlinear, Soft Matter Phys 2007; 75. https://doi.org/10.1103/PhysRevE.75.021915 PMID: 17358375

14. Schroeter MS, Charlesworth P, Kitzbichler MG, Paulsen O, Bullmore ET. Emergence of Rich-Club Topology and Coordinated Dynamics in Development of Hippocampal Functional Networks In Vitro. J Neurosci 2015; 35:5459–70. https://doi.org/10.1523/JNEUROSCI.4259-14.2015 PMID: 25855164

15. Bonifazi P, Goldin M, Picardo MA, Jorquera I, Cattani A, Bianconi G, et al. GABAergic hub neurons orchestrate synchrony in developing hippocampal networks. Science 2009; 326:1419–24. https://doi.org/10.1126/science.1175509 PMID: 19965761

16. Margolis EB, Toy B, Himmels P, Morales M, Fields HL. Identification of Rat Ventral Tegmental Area GABAergic Neurons. PLoS One 2012; 7:e42365. https://doi.org/10.1371/journal.pone.0042365 PMID: 22860119

17. Heysieattalab S, Naghdi N, Hosseinmardi N, Zarrindast MR, Haghparast A, Khoshbouei H. Methamphetamine-induced enhancement of hippocampal long-term potentiation is modulated by NMDA and GABA receptors in the shell–accumbens. Synapse 2016; 70:325–35. https://doi.org/10.1002/syn.21905 PMID: 27029021

18. Padgett CL, Lalive AL, Tan KR, Terunuma M, Munoz MB, Pangalos MN, et al. Methamphetamine-evoked depression of GABA(B) receptor signaling in GABA neurons of the VTA. Neuron 2012; 73:978–89. https://doi.org/10.1016/j.neuron.2011.12.031 PMID: 22405207

19. Runfeldt MJ, Sadovsky AJ, MacLean JN. Acetylcholine functionally reorganizes neocortical microcircuits. J Neurophysiol 2014; 112:1205–16. https://doi.org/10.1152/jn.00071.2014 PMID: 24872527

20. Hiolski EM, Ito S, Beggs JM, Lefebvre KA, Litke AM, Smith DR. Domoic acid disrupts the activity and connectivity of neuronal networks in organotypic brain slice cultures. Neurotoxicology 2016; 56:215–24. https://doi.org/10.1016/j.neuro.2016.08.004 PMID: 27506300

21. Pologruto TA, Yasuda R, Svoboda K. Monitoring neural activity and [Ca2+] with genetically encoded Ca2+ indicators. J Neurosci 2004; 24:9572–9. https://doi.org/10.1523/JNEUROSCI.2854-04.2004 PMID: 15509744

22. Sambo D, Lin M, Richardson B, Jagnarine D, Madhurt S, Owens A, et al. The sigma-1 receptor modulates methamphetamine-dysregulated dopamine neurotransmission. FASEB J 2017; 31:911–86. https://doi.org/10.1038/s41467-017-02087-x

23. Bullmore E, Sporns O. Complex brain networks: graph theoretical analysis of structural and functional systems. Nat Rev Neurosci 2009; 10:186–98. https://doi.org/10.1038/nrn2575 PMID: 19190637

24. Dechery JB, MacLean JN. Functional triplet motifs underlie accurate predictions of single-trial responses in populations of tuned and untuned V1 neurons. PLoS Comput Biol 2018; 14:e1006153. https://doi.org/10.1371/journal.pcbi.1006153 PMID: 29727448

25. Chambers B, MacLean JN. Higher-Order Synaptic Interactions Coordinate Dynamics in Recurrent Networks. PLoS Comput Biol 2016; 12:e1005078. https://doi.org/10.1371/journal.pcbi.1005078 PMID: 27542093

26. Adhikari S, Curtis PD, Adrian AB, Corchado JC, Comeron JM, Adu-Gyamfi R, et al. Epigenetic regulation in Parkinson's disease. Sci Rep 2016; 7:1–8. https://doi.org/10.1016/j.bios.2016.07.082

27. Goodwin JS, Larson GA, Swant J, Sen N, Javitch JA, Zahniser NR, et al. Amphetamine and methamphetamine differentially affect dopamine transporters in vitro and in vivo. J Biol Chem 2009; 284:2978–89. https://doi.org/10.1074/jbc.M805298200 PMID: 19047053

28. Saha K, Sambo D, Richardson BD, Lin LM, Butler B, Villarroel L, et al. Intracellular methamphetamine prevents the dopamine-induced enhancement of neuronal firing. J Biol Chem 2014; 289:22246–57. https://doi.org/10.1074/jbc.M114.563056 PMID: 24962577

29. Lin M, Sambo D, Khoshbouei H. Methamphetamine Regulation of Firing Activity of Dopamine Neurons. J Neurosci 2016; 36:10376–91. https://doi.org/10.1523/JNEUROSCI.1392-16.2016 PMID: 27707972

30. Sambo DO, Lin M, Owens A, Lebowitz J, Richardson B, Jagnarine D, et al. The sigma-1 receptor modulates methamphetamine dysregulation of dopamine neurotransmission. Nat Commun 2017.

31. Surmeier DJ, Obeso JA, Halliday GM. Selective neuronal vulnerability in Parkinson disease. Nat Rev Neurosci 2017; 18:101–13. https://doi.org/10.1038/nrn.2016.178 PMID: 28104909

32. Chen T-W, Wardill TJ, Sun Y, Pulver SR, Renninger SL, Baohan A, et al. Ultrasensitive fluorescent proteins for imaging neuronal activity. Nature 2013; 499:295–300. https://doi.org/10.1038/nature12354 PMID: 23868258

33. Mukamel EA, Nimmerjahn A, Schnitzer MJ. Automated Analysis of Cellular Signals from Large-Scale Calcium Imaging Data. Neuron 2009; 63:747–60. https://doi.org/10.1016/j.neuron.2009.08.009 PMID: 19778505

34. Reznichenko L, Cheng Q, Nizar K, Gratiy SL, Saisan PA, Rockenstein EM, et al. In vivo alterations in calcium buffering capacity in transgenic mouse model of synucleinopathy. J Neurosci 2012; 32:9992–8. https://doi.org/10.1523/JNEUROSCI.1270-12.2012 PMID: 22815513

35. Balkenius A, Johansson AJ, Balkenius C. Comparing Analysis Methods in Functional Calcium Imaging of the Insect Brain. PLoS One 2015; 10:e0129614. https://doi.org/10.1371/journal.pone.0129614 PMID: 26046538

36. Saha K, Sambo D, Richardson BD, Lin LM, Butler B, Villarroel L, et al. Intracellular methamphetamine prevents the dopamine-induced enhancement of neuronal firing. J Biol Chem 2014; 289:22246–57. https://doi.org/10.1074/jbc.M114.563056 PMID: 24962577

37. Vallar L, Meldolesi J. Mechanisms of signal transduction at the dopamine D2 receptor. Trends Pharmacol Sci 1989; 10:74–7. https://doi.org/10.1016/0165-6147(89)90082-5 PMID: 2655242

38. Kravitz A V., Freeze BS, Parker PRL, Kay K, Thwin MT, Deisseroth K, et al. Regulation of parkinsonian motor behaviours by optogenetic control of basal ganglia circuitry. Nature 2010; 466:622–6. https://doi.org/10.1038/nature09159 PMID: 20613723

39. Kravitz A V, Tye LD, Kreitzer AC. Distinct roles for direct and indirect pathway striatal neurons in reinforcement. Nat Neurosci 2012; 15:816–8. https://doi.org/10.1038/nn.3100 PMID: 22544310

40. Krasnova IN, Justinova Z, Ladenheim B, Jayanthi S, McCoy MT, Barnes C, et al. Methamphetamine self-administration is associated with persistent biochemical alterations in striatal and cortical dopaminergic terminals in the rat. PLoS One 2010; 5:e8790. https://doi.org/10.1371/journal.pone.0008790 PMID: 20098750

41. Moszczynska A, Callan SP. Molecular, Behavioral and Physiological Consequences Methamphetamine Neurotoxicity: Implications for Treatment. J Pharmacol Exp Ther 2017; 362:jpet.116.238501. https://doi.org/10.1124/jpet.116.238501 PMID: 28630283

42. Orsini CA, Colon-Perez LM, Heshmati SC, Setlow B, Febo M. Functional Connectivity of Chronic Cocaine Use Reveals Progressive Neuroadaptations in Neocortical, Striatal and Limbic Networks. Eneuro 2018; 5:ENEURO.0081-18.2018. https://doi.org/10.1523/ENEURO.0081-18.2018 PMID: 30073194

43. Colon-Perez LM, Pino JA, Saha K, Pompilus M, Kaplitz S, Choudhury N, et al. Functional connectivity, behavioral and dopaminergic alterations 24 hours following acute exposure to synthetic bath salt drug methylenedioxypyrovalerone. Neuropharmacology 2018; 137:178–93. https://doi.org/10.1016/j.neuropharm.2018.04.031 PMID: 29729891

44. Nephew BC, Febo M, Huang W, Colon-Perez LM, Payne L, Poirier GL, et al. Early life social stress and resting state functional connectivity in postpartum rat anterior cingulate circuits. J Affect Disord 2018; 229:213–23. https://doi.org/10.1016/j.jad.2017.12.089 PMID: 29324369

45. Huang Y, Tsai SJ, Su TW, Sim CB. Effects of Repeated High-Dose Methamphetamine on Local Cerebral Glucose Utilization in Rats. Neuropsychopharmacology 1999; 21:427–34. https://doi.org/10.1016/S0893-133X(99)00029-9 PMID: 10457540

46. Xi Z-X, Kleitz HK, Deng X, Ladenheim B, Peng X-Q, Li X, et al. A single high dose of methamphetamine increases cocaine self-administration by depletion of striatal dopamine in rats. Neuroscience 2009; 161:392–402. https://doi.org/10.1016/j.neuroscience.2009.03.060 PMID: 19336247

47. Krasnova IN, Ladenheim B, Hodges AB, Volkow ND, Cadet JL. Chronic methamphetamine administration causes differential regulation of transcription factors in the rat midbrain. PLoS One 2011; 6:e19179. https://doi.org/10.1371/journal.pone.0019179 PMID: 21547080

48. Gutierrez A, Williams MT, Vorhees C V. A Single High Dose of Methamphetamine Reduces Monoamines and Impairs Egocentric and Allocentric Learning and Memory in Adult Male Rats. Neurotox Res 2018; 33:671–80. https://doi.org/10.1007/s12640-018-9871-9 PMID: 29427284

49. Woodman MM, Jirsa VK. Emergent Dynamics from Spiking Neuron Networks through Symmetry Breaking of Connectivity. PLoS One 2013; 8:e64339. https://doi.org/10.1371/journal.pone.0064339 PMID: 23691200

50. Nowotny T, Rabinovich MI. Dynamical Origin of Independent Spiking and Bursting Activity in Neural Microcircuits 2007. https://doi.org/10.1103/PhysRevLett.98.128106 PMID: 17501162

51. Lautenschläger J, Mosharov E V., Kanter E, Sulzer D, Kaminski Schierle GS. An Easy-to-Implement Protocol for Preparing Postnatal Ventral Mesencephalic Cultures. Front Cell Neurosci 2018; 12:44. https://doi.org/10.3389/fncel.2018.00044 PMID: 29556177

52. Liang X, He Y, Salmeron BJ, Gu H, Stein EA, Yang Y. Interactions between the Salience and Default-Mode Networks Are Disrupted in Cocaine Addiction. J Neurosci 2015; 35:8081–90. https://doi.org/10.1523/JNEUROSCI.3188-14.2015 PMID: 26019326

53. Luo Q, Poelzing S, Tech V, Shaoqun Zeng U, Dubbs alex A, Yuste R, et al. moco: Fast Motion Correction for Calcium Imaging. Front Neuroinformatics | www.Frontiersin.Org 2016; 10. https://doi.org/10.3389/fninf.2016.00006 PMID: 26909035

54. Lim S, Radicchi F, van den Heuvel MP, Sporns O. Discordant attributes of structural and functional brain connectivity in a two-layer multiplex network. Sci Rep 2019; 9:2885. https://doi.org/10.1038/s41598-019-39243-w PMID: 30814615

55. Newman MEJ. Assortative Mixing in Networks. Phys Rev Lett 2002; 89:208701. https://doi.org/10.1103/PhysRevLett.89.208701 PMID: 12443515

56. Onnela J-P, Saramäki J, Kertész J, Kaski K. Intensity and coherence of motifs in weighted complex networks. Phys Rev E 2005; 71:065103. https://doi.org/10.1103/PhysRevE.71.065103 PMID: 16089800